Cell cycle-dependent phosphorylation of PRPS1 fuels nucleotide synthesis and promotes tumorigenesis

Xiaoqian Jing[*1,2,3], Xiong-jun Wang[*4], Tao Zhang[*1], Wencheng Zhu[5], Yi Fang[6], Haoxuan Wu[1,2], Xinyu Liu[7], Ding Ma[8], Xiaopin Ji[1], Yimei Jiang[3], Kun Liu[3], Xianze Chen[1], Yi Shi[1], Yaqi Zhang[1,2], Minmin Shi[2], Weihua Qiu[**1,2], Ren Zhao[**1,2,3]

1. Department of Surgery, Ruijin Hospital, Shanghai Jiao Tong University School of Medicine, Shanghai, 200025, China

2. Shanghai Institute of Digestive Surgery, Ruijin Hospital, Shanghai Jiao Tong University School of Medicine, Shanghai, 200025, China

3. Department of General Surgery, Ruijin North Hospital Shanghai Jiaotong University School of Medicine, Shanghai, 201800, China

4. Precise Genome Engineering Center, School of Life Sciences, Guangzhou University, Guangzhou, 510006, China

5. Shanghai Institute of Biochemistry and Cell Biology, Chinese Academy of Sciences, Shanghai 200031, China

6. Department of Emergency Medicine, Shanghai Tenth People's Hospital, Tongji University School of Medicine, Shanghai, 200072, China

7. Department of Gastrointestinal Surgery, The First Affiliated Hospital of Zhengzhou University, Zhengzhou, Henan 450052, China

8. Central Laboratory, Renji Hospital, School of Medicine, Shanghai Jiaotong University, Shanghai, 200001, China

* Xiaoqian Jing, Xiongjun Wang and Tao Zhang contributed equally to this work.

** Co-Corresponding Author:

Weihua Qiu, M.D., Ph.D.

Department of Surgery Ruijin Hospital, Shanghai Jiao Tong University School of Medicine.197 Rujin Er Road Shanghai, China 200025.

E-mail: drqwh2003@126.com

**Correspondence:

Ren Zhao, M.D., Ph.D.

Department of Surgery Ruijin Hospital, Shanghai Jiao Tong University School of Medicine.197 Rujin Er Road Shanghai, China 200025.

Tel: 86-21-64370045, Ext: 666048

E-mail: zhaorensurgeon@aliyun.com

Running title: PRPS1 phosphorylation promotes tumorigenesis

Key words: PRPS1, CDK1, phosphorylation, cell cycle, colorectal cancer

Financial support: This study was supported by the National Natural Science Foundation of China (NO. 81272751); and the Natural Science Foundation of Shanghai (NO. 18ZR1424300).

Disclosure of Potential Conflicts of Interest

No potential conflicts of interest were disclosed.

Abstract

Nucleotide supply is essential for DNA replication in proliferating cells including cancer cells. Ribose-phosphate diphosphokinase 1 (PRPS1) is a key enzyme to produce the consensus precursor of nucleotide synthesis. PRPS1 participates in the pentose phosphate

pathway (PPP) by catalyzing the phospho-ribosylation of D-ribose 5-phosphate (R-5P) to 5-phosphoribosyl-1-pyrophosphate (PRPP). Therefore, PRPS1 not only controls purine biosynthesis and supplies precursors for DNA and RNA biosynthesis but also regulates PPP through a feedback loop of the PRPS1 substrate R-5P. However, it is still elusive whether PRPS1 enhances nucleotide synthesis during cell cycle progression. In this study, we explore the role and activation mechanism of PRPS1 in cell cycle progression of CRC, and observed a peak in its enzymatic activity during S phase. CDK1 contributes to upregulation of PRPS1 activity by phosphorylating PRPS1 at S103; loss of phosphorylation at S103 delayed the cell cycle and decreased cell proliferation. PRPS1 activity in colorectal cancer samples is higher than in adjacent tissue, and the use of an antibody that specifically detects PRPS1 phosphorylation at S103 showed consistent results in 184 CRC tissues. In conclusion, compared with upregulation of PRPS1 expression levels, increased PRPS1 activity, which is marked by S103 phosphorylation, is more important in promoting tumorigenesis and is a promising diagnostic indicator for CRC.

Significance (Precis)

Findings show that the enzymatic activity of PRPS1 is crucial for cell cycle regulation and suggest PRPS1 phosphorylation at S103 as a direct therapeutic target and diagnostic biomarker for CRC.

Introduction

Colorectal cancer (CRC) is one of the most common human malignancies and ranks third among cancer-related deaths worldwide (1,2). As the global population ages, an increase in the CRC incidence rate is forecasted for the next several decades (3,4). Although the CRC survival rate has improved with enhanced surgical techniques and adjuvant therapy, prognosis

is still dramatically dependent on the stage at diagnosis. Recently, deregulated nucleotide metabolism, especially purine biosynthesis, has been characterized as an important driver of cancer progression (5,6). Although there are numerous connections linking diseases with mutations in nucleotide metabolic enzymes, such as PRPS1 mutations (7,8), post-translational modifications (PTMs) of PRPS1 may also directly influence nucleotide biosynthesis (9,10). However, whether CRC progression is associated with the abnormal activities of nucleotide metabolic enzymes remains unknown.

An obvious correlation exists between nucleotide metabolism and the cell cycle. Sufficient purines can fuel cell cycle progression and maintain DNA fidelity during replication (11). *De novo* purine biosynthesis is the major source of nucleotide metabolism and is often upregulated in cancer cells (12). The pentose phosphate pathway (PPP) is important for glucose metabolism and is considered to have a vital role in tumorigenesis (13,14). The PPP not only provides reduced nicotinamide adenine dinucleotide phosphate (NADPH) for fatty acid synthesis and acts as a balancer of redox status but also supplies ribose for nucleotide synthesis (15,16). PRPS1 participates in the PPP by catalyzing the phospho-ribosylation of R-5P (D-ribose 5-phosphate) to 5-phosphoribosyl-1-pyrophosphate (PRPP). Therefore, PRPS1 not only controls purine biosynthesis and supplies precursors for DNA and RNA biosynthesis but also regulates the PPP through a feedback loop involving the PRPS1 substrate R-5P.

In this study, we revealed that CRC was distinguishable by a significant increase in PRPS1 enzymatic activity, which is compatible with the pathological factors in current clinical parameters. More importantly, the extent of the difference in PRPS1 enzymatic activity between CRC and normal tissues was considerably more apparent than the differences in PRPS1 expression. PRPS1 activity in CRC cells was elevated in the S phase which depends

on CDK1 overactivation. Defective PRPS1 enzymatic activity induced cell cycle arrest and attenuated cell proliferation. PRPS1 phosphorylation at S103 could be a more direct therapeutic target with fewer side effects than the substrates of CDK1 inhibition that are currently used as therapeutic targets. These findings describe a feedback loop mechanism that underlies the distinct PRPS1 enzymatic activity between CRC cells and normal colorectal cells for the development of new therapeutic strategies in clinic.

Materials and methods

Additional experimental procedures are described in the Supporting Information.

Patients and Tissue Specimens

This study was performed in accordance with the principles of the Declaration of Helsinki and approved by the Ethics Committee of Ruijin Hospital, Shanghai Jiao Tong University School of Medicine. From August 2010 to August 2012, 184 patients (Table S1) were recruited into the current study and the written informed consent was obtained from each patient. None of the participants had a history of radiotherapy or chemotherapy prior to surgery. The histological types were independently assigned by at least three pathologists in a double-blinded fashion. The data on these patients, which included their age, sex, smoking history, blood glucose, body weight, and carcinoembryonic antigen (CEA) level, were prospectively collected. Data on operative procedures, pathologies, and complications, including tumor size, operative method, R0 resection, vascular invasion, degree of differentiation, primary tumor grade, lymphatic metastases, nerve involvement and TNM staging (AJCC 2010 edition), were also collected. Follow-up visits were initiated at the fourth week post-surgery, and overall survival (OS) and disease-free survival (DFS) rates were determined based on the follow-up data. Patients were ineligible if they had preoperative

neoadjuvant chemotherapy, a positive surgical margin under microscopic observation or stage IV on TNM. R0 resection required a negative surgical margin >1 mm, as confirmed by post-operative pathological examination.

We quantitatively scored the tissue sections according to the percentage of positive cells and staining intensity. We rated the staining intensity on a scale of 0-3 as follows: 0, negative; 1, weak; 2, moderate; and 3, strong. We assigned the following proportion scores: X indicates that X% of the tumor cells were stained (range, 0-100), and the H-score was obtained using the following formula: 3×percentage of strongly staining signal+2×percentage of moderately staining signal +1×percentage of weakly staining signal, giving a range of 0 to 10. The scores were compared with OS, defined as the time from the date of diagnosis to death or last known date of follow-up.

Cell Culture

HCT116, LoVo and HEK293T cells were purchased from American Type Culture Collection (ATCC, Manassas, VA, USA). HCT116 and HEK293T cells were cultured in DMEM basic supplemented with 10% fetal calf serum while LoVo cells were cultured in F-12 supplemented with 5% fetal calf serum (Gibco, Australian origin). All cell lines were authenticated using short tandem repeat profiling and tested for mycoplasma infection using the MycoTect kit (Invitrogen, Carlsbad, CA, USA). Total RNA was extracted and isolated from tissue samples and cell lines using TRIzol reagent (Invitrogen). Reverse transcription of RNA was performed using the reverse transcription kit (Promega, Beijing, CHN).

Antibodies and Inhibitors

The following antibodies and reagents were used in this study: PRPS1 polyclonal antibody

(PA5-27749) purchased from ThermoFisher; phospho-tyrosine antibody (MAB16761-SP) purchased from R&D systems; antibodies against HA (sc-7392), β–actin (sc-47778) and PCNA (sc-56) purchased from Santa Cruz Biotechnology; monoclonal anti-phospho-serine antibody (P3430) for western blot, anti-Flag M2 antibody (F3165) and M2 FLAG beads (F1804) purchased from Sigma (Sigma-Aldrich Co. LLC); anti-phospho-CDK1-T161 antibody (#9114), phospho-threonine antibody (#9381), phospho-serine/threonine antibody (#9631), phospho-tyrosine mouse mAb (#9411), CDK1 monoclonal antibody (# 33-1800), CDK2 rabbit mAb (#2546), CDK4 rabbit mAb (#12790), CDK6 mouse mAb (#3136) , CDK7 (MO1) mouse mAb (#2916) and CDK9 rabbit mAb (#2316) purchased from Cell Signaling Technology. PRPS2 Antibody (NBP1-57669) purchased from Novus.

The signaling pathways inhibitors used in this study are as follows: MEK inhibitor PD98059 (S1177, Selleckchem), MEK inhibitor U0126 monoethanolate (U120, Sigma), GSK3 Inhibitor SB216763 (ing-sb21, Invivogen), CDKs inhibitor R547 (S2688, Selleckchem), CDKs inhibitor PHA-793887 (S1487, Selleckchem), CDKs inhibitor SNS-032 (S1145, Selleckchem), CDK1inhibitor Ro-3306 (S7747, Selleckchem), Aurora kinase inhibitor AMG 900 (A11066, Adooq bioscience), PKA inhibitor H89 dihydrochloride (Cat. No. 2910, TOCRIS), Akt inhibitor MK-2206 (S1078, Selleckchem), PI3K inhibitor LY294002 (S1105, Selleckchem), PKC inhibitor Go 6983 (S2911, Selleckchem), HDAC inhibitor trichostatin A (S1045, Selleckchem), Sirtuin inhibitor nicotinamide (72340, SIGMA), calf intestinal alkaline phosphatase (CIP) (M0290S, NEB), ADP (A2574, Sigma); and deferoxamine mesylate salt (D9533, Sigma) were also used.

Plasmids Construction and Transfection

The full-length sequence of PRPS1 open reading frame (960 bp, GenBank accession number NC_000023.11) was obtained using high-fidelity PCR with the following primers:

Human PRPS1: Forward 5'- ATGGAATTCGCTAGCGGATCC atgccgaatatcaaaatcttc-3';

Reverse 5'- ATGTCGACCTCGAGTGCGGCCGC ctattataaagggacatggct-3'.

Mouse PRPS1: Forward 5'- ATGGAATTCGCTAGCGGATCC atgccgaatatcaaaatcttc-3';

Reverse 5'- ATGTCGACCTCGAGTGCGGCCGC ttataaaggaacatggctgaa-3'.

The PCR fragment was inserted into pCDH-FLAG or pETM30 by the recombinant method and was confirmed by sequencing identification. For mutation of wild type PRPS1 to the responding mutant, the following primers were utilized:

F (S11A): 5'-atcttcagcggcagcGcccaccaggacttat-3'

R (S11A): 5'-ataagtcctggtgggCgctgccgctgaagat-3'

F (S47A): 5'-gtggaaattggtgaaGCtgtacgtggagagga-3'

R (S47A): 5'-tcctctccacgtacaGCttcaccaatttccac-3'

F (S103A): 5'-gataagaaagataagGCccgggcgccaatctc -3'

R (S103A): 5'-gagattggcgcccggGCcttatctttcttatc-3'

F (S169A): 5'-aactgcactattgtcGcacctgatgctggtg-3'

R (S169A): 5'-caccagcatcaggtgCgacaatagtgcagtt-3'

F (S314A): 5'-gtttcttacctattcGCccatgtccctttata-3'

R (S314A): 5'-tataaagggacatggGCgaataggtaagaaac-3'

To introduce FLAG into the 3' terminus of PRPS1, we designed primers based on a previous report (17). Specifically, the guide RNA sequence (AGTGCTTCTCATACACCTTCAGG) was cloned into the pX330-PRPS1-knockout plasmid with the mCherry fluorescent protein. The oligo sequence used to introduce FLAG tag into endogenous PRPS1 was 5'-attcaccagagggcgccggtgatcttgggatcccccgacgacgtgctcgagtttctgaaggtgtatgagaagcactctgcccagGACTACAAAGACGATGACGACAAGtgagcacctgctctgtctgcatccggagaattgcctctacctggacctttgtctcacacagcagtaccctgac-3'. The oligo sequence used to introduce FLAG tag into endogenous

PRPS2 was 5'- gacatttccatgatcttggccgaagcaatccgaaggacacacaatggggaatccgtgtcctacctgttcagcc atgtcccgctaGACTACAAAGACGATGACGACAAGtaaatccagaatgggaagtgtccagcaagcctactctg acttctgacttgtttttgttttctggatttttagctgtaggtattc-3'

The oligo sequence was inserted into the pCDH-PRPS1 3'Flag Knockin Donor plasmid with puromycin. pX330-PRPS1 and pCDH-PRPS1 were co-transfected into HCT116 or LoVo cells which were seeded at 1.0×10^5/well in a 24-well plate. After 24 h of incubation, the cells were transfected using Lipofectamine 3000. All cells were then collected by flow cytometry sorting using mCherry fluorescence. The sorted HCT116-FLAG-PRPS1 and LoVo-FLAG-PRPS1 cells were purified and maintained in fresh growth medium and collected for western blot assays.

Construction of Stable-Knockdown PRPS1 and Rescued PRPS1 Clones in HCT116-shPRPS1 and LoVo- shPRPS1 Cells

The shPRPS1 sequence 5'-GCTTGTTGCAAATATGCTA-3' was used to knockdown PRPS1 according to a previous report (5). The shPRPS1 sequence was inserted into the pGIPZ vector by the recombination method. The pGIPZ control plasmid was generated with the control oligonucleotide 5'-GCTTCTAACACCGGAGGTCTT-3'. To establish the stable-knockdown PRPS1 clones HCT116-shPRSP1 and LoVo-shPRSP1, pGIPZ-shPRPS1 was transfected into HCT116 and LoVo cells, respectively.

For the PRPS1 expression-rescue study, pCDH-PRPS1 was used as a template. The wild type PRPS1 sequence (PRPS1-WT) was obtained with the following primers:

Forward primer: 5'-gccaaGCTTGTaGCgAAcATGCTAtctgt-3'

Reverse primer: 5'-acagaTAGCATgTTcGCtACAAGCttggc-3'

These two PRPS1 sequences (PRPS1-S47A and PRPS1-S103A) retained the same protein sequence as wild-type PRPS1, with the exception of alteration of the wild type PRPS1 codon. HCT116-shPRSP1 and LoVo-shPRSP1 were re-introduced by PRPS1-WT, PRPS1-S47A, and PRPS1-S103A using Lipofectamine3000. Therefore, wild-type PRPS1 was restored in the HCT116-shPRSP1-PRPS1-WT and LoVo-shPRSP1-PRPS1-WT cell lines. The HCT116-shPRSP1-PRPS1-S47A and LoVo-shPRSP1-PRPS1-S47A cell lines were rescued by PRPS1-S47A transfection. The HCT116-shPRSP1-PRPS1-S103A and LoVo-shPRSP1-PRPS1-S103A rescued cell lines were established by wild type PRPS1.

Measurement of PRPS1 Activity

Upon construction of stable HCT116-FLAG-PRPS1 and LoVo-FLAG-PRPS1 clones, PRPS1 activity was measured as described previously (18,19). Endogenous FLAG-PRPS1 was purified from HCT116 or LoVo cells, eluted by FLAG peptide, and quantified via the Bradford method. FLAG-PRPS1 was incubated in the reaction buffer (50 mM Tris–HCl, pH 7.4, 5 mM $MgCl_2$, 1 mM EDTA, 1 mM dithiothreitol, 32 mM Na_3PO_4, 0.5 mM ATP, 0.15 mM ribose 50-phosphate, and 0.25 mM P1P5-diadenosine pentaphosphate Ap5A) at 37 °C for 15 min. An equal volume of 0.1 M EDTA was used to terminate the reaction.

For tumor tissues, the harvested tissues were added into lysis buffer, and then homogenized and centrifuged at high speed for 10 minutes to remove debris. The PRPS1 in the supernatant was antibody-purified, and the subsequent activity assay of PRPS1 was well established, which was consistent with the above description. Because this method requires a substantial amount of PRPS1 antibody, we tagged the C-terminus of PRPS1 with FLAG, and FLAG-PRPS1 was purified by FLAG M2 beads and eluted by FLAG peptide.

To measure PRPS1 enzymatic activity, the AMP concentration in the reaction mixture was evaluated by the HPLC-based end-point assay. The filtrates were injected into the HPLC with an ion-paired analytical Supelco C18 column (3 mm, 4.6×150 mm) and eluted with 0.2 mM KH_2PO_4 (pH 6) at room temperature, at a flow rate of 1 ml/min. The absorbance of the solution was recorded spectrophotometrically at 254 nm using a microtiter plate reader (Becton-Dickinson). The AMP standard curve was measured in the linear range of 5–20 mM. The intensity of the AMP peak was used to calculate the AMP concentration from the standard curve and evaluate the total enzyme activity. The ratio of each AMP concentration to that of FLAG-PRPS1 was defined as the activity of PRPS1.

CRISPR/Cas9-mediated PRPS1 Knockout in HCT116 Cells

The following three PRPS1 sgRNAs were designed by CRISPOR (20):

sgRNA-1: CGCCGGCGCGCGCCCAGATTGGG

sgRNA-2: AGCCGAGGTCGCCCCCGCCCTGG

sgRNA-3: GCCGCGCTCGTCGTCGACAACGG

Construction and verification were performed according to a well-established protocol (21).

Spectrum Knockdown of CDKs by siRNA

Spectrum knockdown of the CDKs family was performed using siRNA. GenePharma siRNA design software was used to design the siRNA fragments (GenePharma, Shanghai, China). The efficient knockdown sequences targeting human CDKs are as follows:

CDK1 siRNA: 5'-GCTCGCACTTGGCTTCAAA-3';

CDK2 siRNA: 5'- ACAAGAGCGAGAGGTATAC-3';

CDK4 siRNA: 5'-GGCCGACTTCGGTTCCGGTC-3';

CDK6 siRNA: 5'- GCCAGCTAGTTGAGCGCAC-3';

CDK7 siRNA: 5'-AGCGGCAGCTCCCACCAGGAC-3';

CDK9 siRNA: 5'-TGGAGGCGGCCATGGCAAA-3'.

HCT116 cells were grown to 80–90% confluence and subsequently plated on 6-well plates at a density of 8×10^5 cells/well. The cells were divided into seven groups: siCDK1, siCDK2, siCDK4, siCDK6, siCDK7, siCDK9 and negative control (with siRNA constructed from unrelated sequences). Opti-MEM serum-free culture medium (250 μl; Gibco-BRL) and the corresponding siRNA (100 pmol) were added to a 1.5-ml Eppendorf tube, and 250 μl of Opti-MEM and 5 μl of Lipofectamine 3000 were added into a second EP tube. The subsequent transfection procedure was the same as that used for plasmid transfections. The cells were cultured at 37 °C in 5% CO_2 for 48 h and harvested for western blot analysis.

FACS analysis

The cells were starved by serum-free medium for 24 h for synchronization at the G0 phase. Next, the cells were incubated with fresh medium supplemented with 10% serum for an additional amount time (from zero to 24) and collected every two or four hours. After washing with phosphate-buffered saline (PBS), the cells were fixed in ice-cold 70% EtOH for 2 h at 4°C and centrifuged at 2,000 rpm for 5 min, and washed with PBS twice. The cells were then incubated in RNase solution (1 mg/ml) at 37°C for 30 min and stained with propidium iodide (50 μg/ml) for cell cycle analysis (488 nm excitation). A Galios Flow Cytometer (Beckman) was used for pulse processing and collecting cells fluorescing above an emission wavelength of 620 nm, and data were processed with Modfit software (Verity Software House, ME, USA).

Immunoprecipitation and Mass Spectrum Analyses

For immunoprecipitation analyses, HCT116-PRPS1-FLAG and LoVo-PRPS1-FLAG cell lysates (10 mg of protein) derived from the S phase were incubated with the M2 FLAG antibody at 4 °C for 4 h. Immune complexes were washed five times with lysis buffer (Cell Lysis Buffer, Millipore) and supplemented with a complete mini-protease inhibitor cocktail (Roche Applied Science). After boiling in loading buffer (25 mmol/L Tris, pH 6.8, 1% SDS, 5 mmol/L EDTA), samples were subjected to SDS/PAGE (Bio-Rad). SDS/PAGE separated PRPS1-FLAG was cut from the gel and trypsinized into peptides, which were prepared for mass spectrometric analyses. The PRPS1-FLAG sample was heated to 95 °C for 10 min, and 100 ng of sequencing-grade modified trypsin (Promega, Madison, WI, USA) was added. The digestion proceeded overnight at 37 °C, and the products was analyzed by LC-MS/MS on an Obitrap-XL mass spectrometer (Thermo Fisher Scientific, Waltham, MA, USA). Proteins were identified by a database search of the fragment spectra against the National SwissProt protein database (EBI) using Mascot v.2.3 (Matrix Science, London, UK) and Sequest (v.1.20) *via* Proteome Discoverer v.1.3 (Thermo Fisher Scientific). Phosphopeptide matches were analyzed using PhosphoRS implemented in Proteome Discoverer 2.0.

In vitro CDK1 Kinase Assays for PRPS1 Phosphorylation

The Baculovirus purified recombinant His-CDK1 (100 ng) was incubated with bacterially purified GST-PRPS1 (200 ng) with 0.1 ml of kinase buffer (50 mM Tris-HCl pH 7.5, 100 mM KCl, 50 mM $MgCl_2$, 1 mM Na_3VO_4, 1 mM DTT, 5% glycerol and 0.05 mM ATP) at 25 °C for 1 h. The reactions were terminated by the addition of SDS-PAGE loading buffer, and heated to 100 °C. The reaction mixtures were then subjected to SDS-PAGE analyses and detected using the associated antibodies.

Tumor Xenograft Study

All studies involving animals were approved by the Animal Ethics Committee of Ruijin Hospital, Shanghai Jiao Tong University School of Medicine. Five- to seven-week-old female BALB/c nude mice were purchased from the Shanghai Institute of Material Medica, Chinese Academy of Sciences (Shanghai, China). Tumors were initiated by injection of 2×10^6 LoVo stable cell lines of each group, including LoVo-shPRSP1-PRPS1-WT, LoVo-PRPS1-S103A and control cells into the left groins of the nude mice. After 3 weeks, the largest tumor volume was approximately 400 mm^3. The tumors were dissected and snap-frozen for molecular biology analyses. Total proteins were extracted from the tumors to quantify the level of p-S103 by western blot.

Patient-derived Xenograft (PDX) Mouse Models

To evaluate the *in vitro* treatment efficacy of irinotecan on CRC patients with high or low PRPS1 enzymatic activities, 12 tissue samples with high PRPS1 enzymatic activity and 12 tissue samples with low PRPS1 enzymatic activity were randomly selected (if PDX failed, we replenished the group with backup patient tissues to achieve a sample size of 12). The tumor tissues were sliced into pieces that were 2 mm wide, 2 mm long, and 1 mm thick, and then transplanted into the left and right dorsal (details shown in Figure 7G) in the same nude mouse. Each patient's tumor tissues were transplanted into three independent nude mice. When the PDX grew to 5 mm (width or length), it was considered a successful model. 1.9 ng of irinotecan was injected into each nude mouse twice a day for two consecutive times. The tumor volume every three days for two weeks.

Statistical Analyses

Statistical analysis was performed using Statistical Package for the Social Sciences (SPSS) software version 12 for Windows (SPSS Inc., Chicago, IL, USA). All results are presented as

the mean ± standard deviation (SD) unless stated otherwise. Student's t-tests were used to determine the significance of differences between the experimental groups. One-way ANOVA was used to analyze tumor growth data. Kruskal-Wallis statistical analysis was used to compare the patient survival. $p < 0.05$ was considered significant; *$p < 0.05$; **$p < 0.01$; ***$p < 0.001$. Pearson's correlation analyses were used to compare the regression and correlation between two groups.

Results

PRPS1 enzymatic activity is upregulated in CRC

PRPS1 performs an important function in the first step of nucleotide metabolism (Figure 1A). First, we compared PRPS1 mRNA expression in 24 pairs of CRC tissues to that in adjacent normal tissues. As shown in Figure 1B, PRPS1 was slightly upregulated in the CRC samples. Similar results were observed with regard to the protein level in 8 randomly selected pairs of samples (Figure 1C). Because the difference in PRPS1 mRNA and protein levels in clinical samples were small, we further explored the functional enzymatic activity of PRPS1 in the above 24 pairs of clinical samples. To measure PRPS1 enzymatic activity, the AMP concentration in the reaction mixture was evaluated by the HPLC-based end-point assay. The AMP/PRPS1 calculation was performed to show PRPS1 enzymatic activity (Sup Figure 1). The PRPS1 enzymatic activity in normal tissues was significantly lower than that in CRC tissues (Figure 1D). In addition, we examined the correlation between PRPS1 enzymatic activity and clinicopathological features in 184 patients with complete follow-up information, and the results are summarized in Figure 1E. Higher PRPS1 enzymatic activity levels were observed in more advanced CRC cases. Furthermore, comparison of patients with and without CRC recurrence confirmed that PRPS1 enzymatic activity was strongly correlated with CRC recurrence (Figure 1F). Consistently, based on Kruskal-Wallis statistical analysis,

CRC patients with low PRPS1 enzymatic activity presented with higher survival rates than those with high enzymatic activity (Figure 1G). These findings suggest that CRC can be distinguished by a significant increase in PRPS1 enzymatic activity, which is compatible with pathological factors in current clinical parameters.

Upregulation of PRPS1 enzymatic activity mainly depends on cell cycle progression.

The self-promoter controlling two PRPS1-FLAG cell lines were established by inserting the FLAG tag into the PRPS1 3'UTR (Figure 2A). The AMP concentration was dramatically decreased when the *PRPS1* gene was depleted, indicating that PRPS1 was the major enzyme producing AMP (Sup Fig 2A). As shown in Figure 2B, during a complete cell cycle, the PRPS1 enzymatic activities in two cell lines were dramatically enhanced during the S phase. However, there were no obvious changes in PRPS1 protein expression in either cell line (Figure 2C). We also constructed FLAG-tagged PRPS2 in HCT116 cells (Sup Fig 2B) and assayed PRPS2, and no obvious changes in enzymatic activity and protein expression level were observed (Sup Fig 2C and 2D). To further clarify the relationship between PRPS1 and cell cycle progression, the S phase inhibitor deferoxamine was used to block the cell cycle in the G1/S phase. As shown in Figure 2D, treatment of the two cell lines with deferoxamine ameliorated the increased PRPS1 enzymatic activity. It is reasonable that upregulated PRPS1 enzymatic activity supplies additional nucleotide precursors for DNA synthesis. Therefore, these results indicate that cell cycle progression could drive PRPS1 activation.

ADP can restrain PRPS1 enzymatic activity to a low level. To understand the interplay between cell cycle progression and PRPS1 activity, the PRPS1 inhibitor ADP was employed. Our results showed that the upregulation of PRPS1 enzymatic activity may underlie the exit of S phase, and loss of PRPS1 activity might induce cell cycle arrest in the S phase and delay entrance into the G2/M phase (Figure 2E and Sup Fig 2E). Furthermore, we tested the half-

life of HCT116 cells with or without ADP and ADP treatment reduced cell survival (Sup Fig 2F). Consequently, the proliferation of both two cell lines was a remarkably decreased under ADP treatment (Figure 2F). We speculated that PRPS1 may be post-translationally modified during cell cycle progression, which may result in upregulated PRPS1 activity.

Serine phosphorylation at PRPS1 correlates with its dynamic enzymatic activity during cell cycle progression.

To understand how PRPS1 activity is regulated by PTMs, such as phosphorylation and/or acetylation, PRPS1-FLAG was purified from FLAG tagged cells. After treatment with the phosphorylation inhibitor CIP, PRPS1 showed decreased enzymatic activity in both cell lines compared with that in the mock group. Furthermore, inhibition of acetyl removers (histone deacetylase, HDAC) and SIRT failed to influence PRPS1 enzymatic activity (Figure 3A). Thus, phosphorylation rather than acetylation at PRPS1 is essential for PRPS1 activity regulation.

As shown in Figure 3B, phosphorylation changes at serine and threonine residues were obvious, while tyrosine residues were not altered during the S phase in PRPS1-FLAG. Because serine and threonine have similar residue side chains for the covalent linkage of a phosphate group, anti-serine and anti-threonine antibodies were employed to pinpoint the phosphorylated residue in PRPS1-FLAG. As shown in Figure 3C, a serine peak but not that of threonine phosphorylation, was observed on PRPS1 in the S phase at 14 and 16 h. Interestingly, a threonine phosphorylation peak appeared at 24 h, a G2/M phase time point. A previous report showed that Thr (T) 225 was phosphorylated by KHK-A (9).

We further attempted to identify which serine site contributes to PRPS1 phosphorylation.

PRPS1 purified from LoVo-PRPS1-FLAG cells during the S phase was subjected to mass spectrometry analysis, and protein 3D structure analyses identified five serine phosphorylation sites on PRPS1 during the S phase: S11, S47, S103, S169, and S314 (Figure 3D). Next, these five serine sites were mutated to alanine using site-directed mutagenesis. Using immunoprecipitation and a specific antibody against phosphorylated serine, only S47 and S103 were shown to be phosphorylated in the S phase (Figure 3E and Sup Fig 3). In addition, phosphorylation of the S47 and S103 peptides was confirmed quantitatively, as shown in Figure 3F. Thus, S47 and/or S103 may play the vital role in PRPS1 phosphorylation. Furthermore, we compared the functional difference in enzymatic activity between the S47A and S103A mutations. As shown in Figure 3G, only S103A could block PRPS1 enzymatic activity in the S phase, while S47A had no obvious effect on enzymatic activity.

Functional mapping of PRPS1 S103A mutant in CRC cell lines

Wild type S103 and S103A PRPS1 were transfected into two cell lines (Figure 4A). As shown in Figure 4B and 4C, transfection of the S103A mutant resulted in 50% reductions in the glucose consumption and cellular ATP levels in both rescued cell lines compared to those in the wild-type cell lines (p=0.0027 and 0.0011, respectively). Similar results were observed in LoVo-shPRPS1 cells (p=0.0085 and 0.0036, respectively). Cell cycle analysis showed that the PRPS1 S103A mutant cells were partially arrested in the S phase, which might have been caused by lack of nucleotide synthesis. Specifically, 39.56% of the PRPS1 S103A cells were arrested at 16 h, which represents the S phase, while 28.13% of the PRPS1 WT cells were observed in the S phase (p=0.0017, Figure 4D and Sup Fig 4). Consistently, cell division in the S103A was group significantly decreased, suggesting that the loss of PRPS1 enzymatic activity in the S phase inhibited cell growth (Figure 4E). Conclusively, functional mapping of

the PRPS1 S103A mutation showed that PRPS1 enzymatic activity was the specific pivot for passing the S phase by upregulaing nucleotide synthesis.

CDK1 is required for PRPS1 phosphorylation at S103

An antibody specifically targeting S103 phosphorylation was designed in our lab and prepared by the Abclonal company (Wuhan, China). First, Western blot was used to confirm the specificity of our newly established antibody recognizing PRPS1 S103 phosphorylation in the S phase, and the dot blot result was used as the positive control (Figure 5A and 5B). We confirmed PRPS1 S103 phosphorylation with an oscillation during the cell cycle progression, which was consistent with the results shown in Figure 2B and Figure 3C (Figure 5C).

Multiple serine/threonine kinase inhibitors were applied to discover which kinase is required for phosphorylating PRPS1 at S103. Among the kinase inhibitors against ERK, MEK, GSK3beta, CDK, Aurora 1, PKA, Akt, PI3K, and PKC, only CDK family inhibitors (R547, PHA-793887, and SNS-032) exerted an apparent inhibitory effect on S103 phosphorylation. Aurora 1, also named Aurora B, functions in attachment of the mitotic spindle to the centromere; its expression peaks a maximum at the G2/M transition; while its activity peaks during mitosis. Inhibition of Aurora B attenuated cell cycle progression, which in turn decreased pS103 (Figure 5D). The ERK inhibitor (PD98059) significantly decreased the phosphorylation of PRPS1. As reported previously, ERK functions upstream of CDKs (22), and we speculated that this regulation might be indirect. These results indicated that the CDKs could contribute to the important regulation of PRPS1 phosphorylation and enzymatic activity.

Because the CDK protein kinase family contains at least nine members, we further

pinpointed the individual CDK required for phosphorylating PRPS1 S103. Six important CDK coding genes were knocked down by siRNA (Sup Fig 5). Among them, only CDK1 knockdown apparently inhibited PRPS1 S103 phosphorylation (Figure 5E). As shown in Figure 5F, compared with that achieved by overexpressing the dominant-negative CDK1, the overexpression of WT CDK1 enhanced PRPS1 S103 phosphorylation even in the G1 phase. In addition, the *in vitro* kinase assay revealed a close relationship between CDK1 and PRPS1 S103 phosphorylation, and CDK1 was the specific trigger PRPS1 phosphorylation at S103 (Figure 5G and 5H).

Phosphorylation at S103 is required for *CCND1* expression and tumorigenesis.

The effect of the PRPS1 S103A mutation on CRC cell proliferation was evaluated in paired PRPS1 knockdown and rescue models *in vitro* and *in vivo*. As shown in Figure 6A, both rescued cell lines proliferated at rates similar to that of the control knockdown group (shNT cells). The S103A cell lines exhibited a decreased cell proliferation rate, which was approximately half that of the shPRPS1-rPRPS1-WT cells. Similar results were observed in the colony formation assay, as the colony number was lower in S103A mutant cells than in control cells (Figure 6B). We used CRISPR/Cas9 to knockout (KO) *PRPS1* in HCT116 cells, re-introduced PRPS1-WT or PRPS1-S103A into KO cells, and used the CCK8 assay to demonstrated that PRPS1-S103 phosphorylation is required for CRC cell proliferation (Sup Fig 6A and 6B). The transwell assay showed that PRPS1-S103 phosphorylation was unaffected by loss of PRPS1 enzymatic activity caused by the S103A muation, although complete depletion of PRPS1 slightly reduced metastatic capacity of LoVo cells (Sup Fig 6C). Thus, the PRPS1 S103A mutation resulted a significantly lower proliferation rates of both mutant cell lines compared to that of wild-type cells. Furthermore, overexpressing PRPS2 did not compensate for the depletion of PRPS1 in LoVo cells (Sup Fig 6D and 6E).

Given that decreased phosphorylation at S103 induced cell cycle arrest in the S phase, we speculated that altered PRPS1 enzymatic activity could also alter the cell cycle. *CCND1*, encoding the cyclin-D1 protein, specifically accelerated cell cycle progression from the G1 phase to the S phase. In Figure 6C, *CCND1* expression in the S103A mutant cells was low and displayed a delayed smaller peak compared to that of WT cells. We measured cell proliferation using an inhibitor of CDK1 and revealed that the CDK1 inhibitor had a greater effect on cell proliferation and *CCND1* expression than the S103A mutation (Sup Fig 6F and 6G). As CDK1 has a wide range of substrates (23), this result was most likely due to the inhibition of other CDK1 substrates.

In the *in vivo* assay, LoVo-shPRPS1-PRPS1-WT and LoVo-shPRPS1-PRPS1-S103A were implanted into the right flank of athymic nude mice. Three weeks later, the tumor volume in the LoVo-shPRPS1-PRPS1-WT group was significantly larger than that in the LoVo-shPRPS1-PRPS1-S103A group (Figure 6D). Furthermore, we performed immunohistochemistry (IHC) staining of dissected tumors with an anti-Ki67 antibody, which revealed that tumor cells rescued with rPRPS1 S103A had the reduced growth rate compared to those rescued with rPRPS1 WT (Figure 6E and 6F). To confirm the key role of PRPS1 phosphorylation at S103, three forehand tumor samples from each group were collected and examined by western blot. Consistent with the faster tumor growth, tumor samples from the LoVo-shPRPS1-rPRPS1-WT group exhibited remarkable phosphorylation, while tumors in the LoVo-shPRPS1-rPRPS1-S103A group failed to show PRPS1 phosphorylation and had lower weights (Figure 6G). Furthermore, we performed a tumor-bearing experiment. Fourteen days after inoculation, mice were injected with or without irinotecan (1.9 ng/each mouse, every two days), a CDK1 inhibitor (5 ng/each mouse, every two days) via tail vein.

Simultaneous injection of the CDK1 inhibitor and irinotecan resulted in much better tumor inhibition compared that achieved with the CDK1 inhibitor or irinotecan alone (Sup Fig 6H). The H2AX phosphorylation and caspase 3 cleavage levels in rPRPS1-S103A mutant cells were significantly increased compared to that in rPRPS1-WT cells, indicating that the DNA damage and apoptosis in in these cells were more prominently affected (Sup Fig 6I). We assessed the expression of the *RB* and *E2F1* genes by qRT-PCR. Compared to that in mice containing reintroduced PRPS1-WT HCT116-PRPS1 KO cells, *E2F1* expression in mice containing reintroduced PRPS1-S103A cells was dramatically reduced, but *RB* expression was not obviously different between the two types of mice (Sup Fig 6J). Conclusively, PRPS1 phosphorylation at S103 plays an important role in promoting CRC tumor growth.

PRPS1 S103 phosphorylation tightly correlates with CRC progression in clinical cases

IHC analyses of human CRC specimens were performed with the indicated antibodies in the presence or absence of specific blocking peptide, to prove the specificity of antibody against PRPS1 phosphorylation at S103 (Sup Fig 7A). We confirmed the requirement of CDK1 in PRPS1 phosphorylation at S103; however, CDK1 activation required phosphorylation at T161. Therefore, IHC was employed to further define the clinical relevance of PRPS1-S103 phosphorylation and CDK1-Thr161 phosphorylation (Figure 7A), which showed a positive correlation. Quantitatively, S103 phosphorylation positively correlated with CDK1-T161 phosphorylation (r=0.752, p=0.0019, Figure 7B). Additionally, S103 phosphorylation was positively correlated with PRPS1 enzymatic activity (r=0.690, p=0.0001, Sup Fig 7B). We analyzed the correlation between patient survival and the PRPS1 protein levels in CRC tissues yielding a p value=0.0315 (Sup Fig 7C). Consistently, the ratio of PRPS1-pS103 to total PRPS1 protein showed much more significance (Sup Fig 7D). At follow-up, we compared the survival times of 184 patients with a low staining (score, 0–5) or a high

staining (score, 5.1–10) S103 phosphorylation. Compared to that of patients with low PRPS1 S103 phosphorylation, the median survival of patients with high levels of S103 phosphorylation was significantly lower (p=0.0027, Figure 7C). Further comparison showed that the level of S103 phosphorylation in stage II CRC patients (n=77) was substantially lower than that in stage IV patients (n=9) (p=0.0015, Figure 7D).

The patients with higher recurrence rates presented with higher S103 phosphorylation levels (p=0.0049, Figure 7E). Furthermore, S103 phosphorylation was also associated with patient age, and younger CRC patients potentially had higher phosphorylation levels (Figure 7F). Besides, the PDX model showed that CRC tumors with low S103 phosphorylation presented stronger resistance to irinotecan treatment while CRC tumors with high S103 phosphorylation displayed sensitivity to irinotecan (Figure 7G). These results reveal a relationship between cell cycle progression-dependent PRPS1 S103 phosphorylation and the clinical aggressiveness of CRC. Finally, we concluded our study with a simple model that details how PRPS1 is phosphorylated by CDK1 at S103 upon entering the S phase. In turn, phosphorylated PRPS1 promotes purine biosynthesis and cell cycle progression. The positive feedback loop facilitates tumor cells passing over the cell cycle check point and ensures that they survive chemotherapy, suggesting that disruption of this positive feedback loop could be a potential therapeutic strategy for tumor cells (Figure 7H).

Discussion

PRPSs catalyze the phosphoribosylation of R-5P, the starting substrate of *de novo* purine synthesis to PRPP, which is essential for the synthesis of purine and pyrimidine nucleotides, as well as the pyridine nucleotide cofactors NAD and NADP and the amino acids histidine and tryptophan (24). However, the enzymatic activities of PRPSs, which are regulated by

PTMs during cell cycle progression, are primarily unknown. Three human PRPSs have been identified: PRPS1 and PRPS2, which are widely expressed in many tissues, and PRPS3, which is expressed specifically in the testis (24,25). Despite having only 6% amino acid sequence diversity, the enzymatic activities of PRPS1 and PRPS2 largely differ in their regulation. The activity of PRPS1 is kept low by end-product feedback inhibition, while PRPS2 displays low feedback insensitivity (26,27). Mutations that enhance PRPS1 activity are tightly correlated with many diseases, such as hyperuricemia, gout and nonsyndromic X-linked sensorineural deafness (8). Recently, more malignant diseases, such as relapsed childhood acute lymphoblastic leukemia (7), glioblastoma (28), breast cancer (29), and hepatocellular carcinoma (9), have been related to PRPS1 mutation or PRPS1 PTMs. In this study, we showed that the enzymatic activity of PRPS1 was positively correlated with CRC progression. Despite the tight correlation between PRPS1 and the cell cycle, the detailed mechanism underlying the switch from purine metabolic disorders to tumorigenesis needs to be clarified.

Two layers exist regarding the regulation of an enzyme: 1) the enzymatic quantity, including the levels of mRNA and protein; and 2) the enzymatic activity, which is regulated by mutations or PTMs. Although both PRPS1 expression and enzymatic activity were increased in CRC tissues compared with those in adjacent tissues, the upregulated PRPS1 enzymatic activity was more important. PRPS1 activity is regulated by phosphorylation and allostery (10) and ADP is the key allosteric inhibitor of PRPS at low concentrations of the substrate R-5P (27,30). Here, PRPS1 enzymatic activity restricted by ADP arrested the cell cycle in the S phase, leading a remarkably decreased proliferation of CRC cells. Furthermore, we found that the PRPS1 enzymatic activity, rather than the PRPS1 quantity, mainly contributed to the promotion of CRC cell cycle progression. Based on these results, we hypothesized that

PRPS1 PTMs occur during cell cycle progression, which may result in conformational and enzymatic changes in PRPS1.

The accurate cell cycle transition from the G1 phase to the S phase is crucial for eukaryotic cell proliferation control, and its deregulation may promote carcinogenesis (31). Unscheduled proliferation and genomic instability have been frequently observed in tumor cells (32). In this study, PRPS1 functions as a CDK1 substrate in the G1/S transition and can be phosphorylated at S47 and S103. S103 phosphorylation can upregulate the PRPS1 activity from low to high, and more importantly, phosphorylation of S103 can induce PRPS1 a conformational change in PRPS1 from a closed to open state, such that its easily accessed by of R-5P phosphoribosylation (7). Conclusively, functional mapping of the PRPS1 S103A mutation showed PRPS1 enzymatic activity to be the specific pivot point for surpassing the S phase by upregulating nucleotide synthesis.

CDKs control the mammalian cell cycle, and the interplay between CDK1 and PRPS1 results in positive feedback to promote CRC development (33). In this study, we revealed that the level of CDK1 phosphorylation at T161 was positively correlated with that of PRPS1 at S103, which indicates that CDK1-driven tumor cell proliferation partially depends on PRPS1 phosphorylation at S103. Emerging evidence suggests that tumor cells may also utilize individual CDKs to satisfy the specific needs under different conditions. Therapeutic strategies based on CDK inhibition should take into consideration the metabolic state of tumor cells. However, the side effects of CDKs as cancer targets are challenging, and some problems have been associated with the clinical applications of current CDK inhibitors. Thus, it is essential to discover additional details regarding the associations between CDKs and their substrates, such as where and when CDKs phosphorylate their substrates and under

what conditions. It is on this premise that disrupting the associations between CDKs and their substrates could be a good strategy for designing specific antineoplastic agents. Irinotecan is a DNA topoisomerase I inhibitor that inhibits DNA synthesis and causes cell cycle arrest at S phase. Therefore, targeting cell cycle progression combined with CDK inhibitors could be a novel therapeutic strategy for CRC.

In conclusion, our study links purine biosynthesis during nucleotide metabolism with cell cycle progression, revealing that cell cycle-promoted CDK1 kinase activity positively drives cell cycle progression by phosphorylating PRPS1 at S103. The precise upregulation of PRPS1 enzymatic activity in the S phase confers tumor cells the ability to bypass the cell cycle checkpoint. Therefore, manipulation of S103 phosphorylation would be a promising strategy to arrest CRC. Notably, the S103N and S103T mutations have been shown to affect PRPS1 enzyme activity in acute lymphocytic leukemia patients (7). S103 functions in the binding of GDP or ADP to allosteric sites A and B. PRPS1 phosphorylation at S103 could also block the binding of ADP to PRPS1. Based on current knowledge, a substantial amount of work must be performed before targeting a specific PRPS1 phosphorylation site can be utilized for therapeutic purposes. As a prognostic biomarker, PRPS1 pS103 can predict the survival and recurrence of CRC patients. In light of our data showing that the combination of CDK and DNA topoisomerase I inhibitors showed descried therapeutic effect on PDX with high PRPS1 pS103, we think that establishing PRPS1 S103 phosphorylation is more likely to be a diagnostic biomarker guiding precision medicine in clinic.

References

1. Siegel R, DeSantis C, Virgo K, Stein K, Mariotto A, Smith T*, et al.* Cancer treatment and survivorship statistics, 2012. CA: a cancer journal for clinicians **2012**;62:220-41
2. Jemal A, Bray F, Center MM, Ferlay J, Ward E, Forman D. Global cancer statistics. CA: a cancer journal for clinicians **2011**;61:69-90
3. Zeng H, Zheng R, Zhang S, Zuo T, Xia C, Zou X*, et al.* Esophageal cancer statistics in China, 2011: Estimates based on 177 cancer registries. Thoracic cancer **2016**;7:232-7

4. Chen W. Cancer statistics: updated cancer burden in China. Chinese journal of cancer research = Chung-kuo yen cheng yen chiu **2015**;27:1
5. Qiu Z, Guo W, Wang Q, Chen Z, Huang S, Zhao F*, et al.* MicroRNA-124 reduces the pentose phosphate pathway and proliferation by targeting PRPS1 and RPIA mRNAs in human colorectal cancer cells. Gastroenterology **2015**;149:1587-98 e11
6. DeBerardinis RJ, Lum JJ, Hatzivassiliou G, Thompson CB. The biology of cancer: metabolic reprogramming fuels cell growth and proliferation. Cell metabolism **2008**;7:11-20
7. Li B, Li H, Bai Y, Kirschner-Schwabe R, Yang JJ, Chen Y*, et al.* Negative feedback-defective PRPS1 mutants drive thiopurine resistance in relapsed childhood ALL. Nature medicine **2015**;21:563-71
8. Mittal R, Patel K, Mittal J, Chan B, Yan D, Grati M*, et al.* Association of PRPS1 Mutations with Disease Phenotypes. Disease markers **2015**;2015:127013
9. Li X, Qian X, Peng LX, Jiang Y, Hawke DH, Zheng Y*, et al.* A splicing switch from ketohexokinase-C to ketohexokinase-A drives hepatocellular carcinoma formation. Nature cell biology **2016**;18:561-71
10. Qian X, Li X, Tan L, Lee JH, Xia Y, Cai Q*, et al.* Conversion of PRPS hexamer to monomer by AMPK-mediated phosphorylation inhibits nucleotide synthesis in response to energy stress. Cancer discovery **2017**
11. Ben-Sahra I, Howell JJ, Asara JM, Manning BD. Stimulation of de novo pyrimidine synthesis by growth signaling through mTOR and S6K1. Science **2013**;339:1323-8
12. Tong X, Zhao F, Thompson CB. The molecular determinants of de novo nucleotide biosynthesis in cancer cells. Current opinion in genetics & development **2009**;19:32-7
13. Patra KC, Hay N. The pentose phosphate pathway and cancer. Trends in biochemical sciences **2014**;39:347-54
14. Ying H, Kimmelman AC, Lyssiotis CA, Hua S, Chu GC, Fletcher-Sananikone E*, et al.* Oncogenic Kras maintains pancreatic tumors through regulation of anabolic glucose metabolism. Cell **2012**;149:656-70
15. Du W, Jiang P, Mancuso A, Stonestrom A, Brewer MD, Minn AJ*, et al.* TAp73 enhances the pentose phosphate pathway and supports cell proliferation. Nature cell biology **2013**;15:991-1000
16. Jiang P, Du WJ, Wang XW, Mancuso A, Gao XA, Wu MA*, et al.* p53 regulates biosynthesis through direct inactivation of glucose-6-phosphate dehydrogenase. Nature cell biology **2011**;13:310-U278
17. Platt RJ, Chen S, Zhou Y, Yim MJ, Swiech L, Kempton HR*, et al.* CRISPR-Cas9 knockin mice for genome editing and cancer modeling. Cell **2014**;159:440-55
18. Micheli V, Rocchigiani M, Pompucci G. An HPLC-linked assay of phosphoribosylpyrophosphate synthetase activity in the erythrocytes of adults and children with neurological disorders. Clinica chimica acta; international journal of clinical chemistry **1994**;227:79-86
19. Zhang F, Patel DM, Colavita K, Rodionova I, Buckley B, Scott DA*, et al.* Arginylation regulates purine nucleotide biosynthesis by enhancing the activity of phosphoribosyl pyrophosphate synthase. Nature communications **2015**;6:7517
20. Haeussler M, Schonig K, Eckert H, Eschstruth A, Mianne J, Renaud JB*, et al.* Evaluation of off-target and on-target scoring algorithms and integration into the guide RNA selection tool CRISPOR. Genome Biol **2016**;17:148
21. Ran FA, Hsu PD, Wright J, Agarwala V, Scott DA, Zhang F. Genome engineering using the CRISPR-Cas9 system. Nat Protoc **2013**;8:2281-308
22. Chambard JC, Lefloch R, Pouyssegur J, Lenormand P. ERK implication in cell cycle regulation. Biochim Biophys Acta **2007**;1773:1299-310
23. Holt LJ, Tuch BB, Villen J, Johnson AD, Gygi SP, Morgan DO. Global analysis of Cdk1 substrate phosphorylation sites provides insights into evolution. Science **2009**;325:1682-6
24. Hove-Jensen B. Mutation in the phosphoribosylpyrophosphate synthetase gene (prs) that results in simultaneous requirements for purine and pyrimidine nucleosides, nicotinamide nucleotide, histidine, and tryptophan in Escherichia coli. Journal of bacteriology **1988**;170:1148-52
25. Taira M, Iizasa T, Yamada K, Shimada H, Tatibana M. Tissue-differential expression of two distinct genes for phosphoribosyl pyrophosphate synthetase and existence of the testis-specific transcript. Biochimica et biophysica acta **1989**;1007:203-8
26. Nosal JM, Switzer RL, Becker MA. Overexpression, purification, and characterization of recombinant human 5-phosphoribosyl-1-pyrophosphate synthetase isozymes I and II. The Journal of biological chemistry **1993**;268:10168-75
27. Li S, Lu Y, Peng B, Ding J. Crystal structure of human phosphoribosylpyrophosphate synthetase 1 reveals a novel allosteric site. The Biochemical journal **2007**;401:39-47

28. Wang X, Yang K, Xie Q, Wu Q, Mack SC, Shi Y*, et al.* Purine synthesis promotes maintenance of brain tumor initiating cells in glioma. Nature neuroscience **2017**;20:661-73
29. He M, Chao L, You YP. PRPS1 silencing reverses cisplatin resistance in human breast cancer cells. Biochemistry and cell biology = Biochimie et biologie cellulaire **2017**;95:385-93
30. Eriksen TA, Kadziola A, Bentsen AK, Harlow KW, Larsen S. Structural basis for the function of Bacillus subtilis phosphoribosyl-pyrophosphate synthetase. Nature structural biology **2000**;7:303-8
31. Massague J. G1 cell-cycle control and cancer. Nature **2004**;432:298-306
32. Kastan MB, Bartek J. Cell-cycle checkpoints and cancer. Nature **2004**;432:316-23
33. Malumbres M, Barbacid M. Mammalian cyclin-dependent kinases. Trends in biochemical sciences **2005**;30:630-41

Figure and Figure Legends

Figure 1. PRPS1 enzymatic activity is upregulated in colorectal cancer.

A, PRPS1/2 catalyzing the reaction of ribose-5-phosphate (R5P) with ATP to yield PRPP (5-phosphoribosyl-a-1-pyrophosphate) and AMP, links the pentose phosphate pathway to the pyrimidine and purine nucleotide *de novo* and salvage pathways.

B, C & D PRPS1 mRNA expression (B), protein level (C) and enzymatic activity (D) in clinical colorectal cancer and adjacent tissues. Twenty-four pairs of colorectal cancers and their adjacent tissues were analyzed for mRNA expression and enzymatic activity, and 8 pairs of samples were analyzed for protein level detection. β–actin was used as an internal control. The difference in PRPS1 enzymatic activity was detected in the presence of phosphate (25 mM) and calculated based on AMP levels, normalized to PRPS1 protein levels. Ad, adjacent tissues; Tu, tumor tissues.

E, PRPS1 enzymatic activity in tumors from grade II to grade IV.

F, PRPS1 enzymatic activity in tumors derived from patients with or without recurrence.

G, Colorectal cancer patient survival was correlated with the PRPS1 enzymatic activity in their tumors.

Figure 2. Upregulation of PRPS1 enzymatic activity depends mainly on cell cycle progression.

B, D, E, the data represent the mean ± SD from three independent experiments.

A, Construction of endogenous FLAG-tagged PRPS1 in HCT116 and LoVo cells. The FLAG tag was inserted into the 3'UTR of *PRPS1*.

B, Dynamic oscillation of PRPS1 enzymatic activity in HCT116 cells and LoVo cells throughout the entire cell cycle.

C, Cells were synchronized in the G0 phase for over 4 h and then released into fresh medium.

The cells were collected at different time points, and detected by immunoblotting.

D, Inhibition of PRPS1 enzymatic activity by the S phase inhibitor deferoxamine (DFOA).

E and **F**, Cell cycle progression and proliferation were inhibited by ADP.

Figure 3. Serine phosphorylation of PRPS1 is correlated with its dynamic enzymatic activity during cell cycle progression.

A, CIP (50 nM) treatment of the FLAG antibody-immunoprecipitated PRPS1 decreased its enzymatic activity. CIP, calf intestinal alkaline phosphatase. H+S, HDAC and SIRT inhibitors: TSA (5 μM) and NAM (50 mM), respectively. Treatment time, half an hour.

B, Elevated serine/threonine phosphorylation of PRPS1 in the S phase. FLAG-PRPS1 was purified from HCT116-PRPS1-FLAG cells during the S phase.

C, Dynamic modifications of serine and threonine phosphorylation during the HCT116 cell cycle. PCNA expression marks S phase progression.

D and E, Mass spectrometry analysis and site mutational analyses of serine phosphorylation in FLAG-PRPS1. **D**, Phospho-serine in the S phase was discovered by mass spectrometry; the 2D structure of PRPS1 determined using Pymol is shown.

E, Phosphorylation of PRPS1 at both S47 and S103 occur in the S phase. FLAG antibody-immunoprecipitated PRPS1 was evaluated.

F, Mass spectrometry analysis of a tryptic fragment at m/z 1007.80 (mass error, 2.94 ppm) matched to the doubly charged peptide 101-DKpSRAPISA-109; the result suggests that S103 was phosphorylated. With regard to phospho-S103, the Sequest score for this match was Xcorr=2.57, the Mascot score was 69, and the expectation value was 7.5×10^{-4}. The presence of b_3^{2+} at 411.38 and y_7^{2+}at 763.82 indicates that the S103 residue was phosphorylated. The probability of phospho-S103 was 96.29%.

G, Enzymatic activity of the PRPS1 S47A and S103A mutants. PRSP1-FLAG vectors

(including WT, S47A and S103A) were transiently transfected into HCT116 or LoVo cells.

Figure 4. PRPS1 S103 phosphorylation was required for cell cycle progression.

B and E, the data represent the mean ± SD from three independent experiments.

A, The generation of HCT116- and LoVo-derived stable cell lines.

B and C, The cells in panel A were used to detect glucose uptake and the cellular ATP level.

D, Cell cycle analysis. shNT cells, shPRPS1 with rPRPS1 WT or S103A cells were arrested by nocodazole (5 μM) at the G2/M phase and released for the indicated time points.

E, BrdU staining assay and statistical analysis.

Figure 5. CDK1 phosphorylates PRPS1 at S103.

A and B, Preparation and specific efficiency assessment of the antibody against phosphorylated S103.

A, Dot blot assay. Gradient increased peptides (from 0 to 500 ng/μl) with or without phosphorylated S103 were blotted with the antibody against phosphorylated S103.

B, PRPS1-FLAG (including WT and S103A mutant) were purified from HCT116 cells and then blotted using the indicated antibodies.

C, The phosphorylation level of PRPS1-S103 was detected during cell cycle progression.

D, Screening of serine kinase inhibitors.

E, siRNA targeting CDKs verified that CDK1 is required for phosphorylating PRPS1 at S103.

F, Overexpression of HA-CDK1 (WT or DN mutant) in HCT116-PRPS1-FLAG cells. DN, dominant negative, impaired most of CDK1 kinase activity.

G, The *in vitro* kinase assay was performed by mixing commercial His-CDK1 (0.5 μg), bacteria-purified GST-PRPS1 WT or S103A (2 μg) and ^{32}P-labeled ATP.

H, The *in vitro* kinase assay was performed by mixing commercial His-CDK1 (0.5 μg) and bacteria-purified GST-PRPS1 WT or S103A (2 μg).

Figure 6. PRPS1 phosphorylation at S103 is required for tumor cell growth by promoting CCND1 gene expression.

A-D, The data represent the mean ± SD from three independent experiments. (*p<0.05; **p<0.01).

A, The cell number was examined using trypan blue staining.

B, Colony-formation assay.

C, *CCND1* gene expression at the indicated time points.

D-G, Xenograft study. LoVo cells stably expressing shNT or shPRPS1 were rescued with rPRPS1 WT or S103A and injected into the groin of randomized nude mice (n=7). The tumor images are presented (D, left panel), and the tumor volumes were quantified (D, right panel). E and F, Ki67 staining of xenograft samples and statistics. Scale bar: 50 μm. G, Examination of PRPS1 pS103 in xenograft samples.

Figure 7. PRPS1 phosphorylation at S103 is correlated with CRC patient survival, phase and prognosis.

A, Representative images of 4 CRC specimens.

B, Semiquantitative scoring was performed (Pearson product moment correlation test). Note that some of the dots on the graphs represent more than one specimen.

C, The survival of 57 patients with low staining scores (0-150; green curve) and 127 patients with high staining scores (151-300; red curve), and their PRPS1 pS103 levels (low staining, n=57; high staining, n=127) were analyzed. Semiquantitative scoring (using a scale from 0 to 300) was performed.

D, Levels of PRPS1 pS103 in the CRC patients in stage II and stage IV. A total of 77 CRC specimens from patients with AJCC stage II cancer and 9 CRC specimens from patients with AJCC stage IV cancer were stained.

E, Levels of PRPS1 pS103 in CRC patients with or without recurrence (0, without recurrence; 1, recurrence).

F, Correlation between PRPS1 pS103 and CRC patient ages.

G, Tumor tissues with low PRPS1 pS103 levels (n=12) and high PRPS1 pS103 levels (n=12) were collected and transplanted into the left and right dorsal regions of nude mice, respectively. Irinotecan, 1.9 ng/each mouse, two injections.

H, The interplay mechanism of PRPS1-S103 phosphorylation and cell cycle progression.

Figure 1

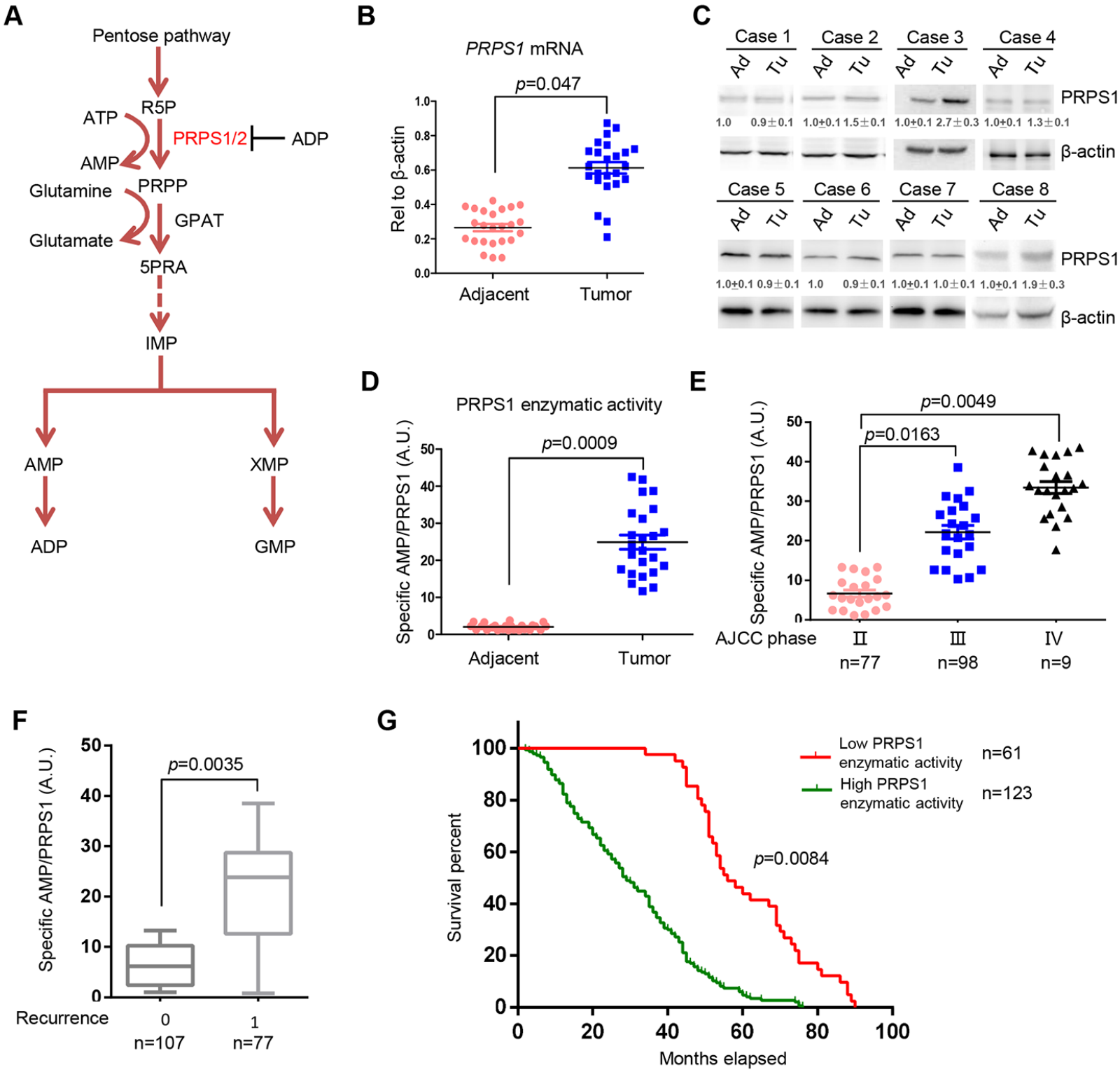

Figure 2

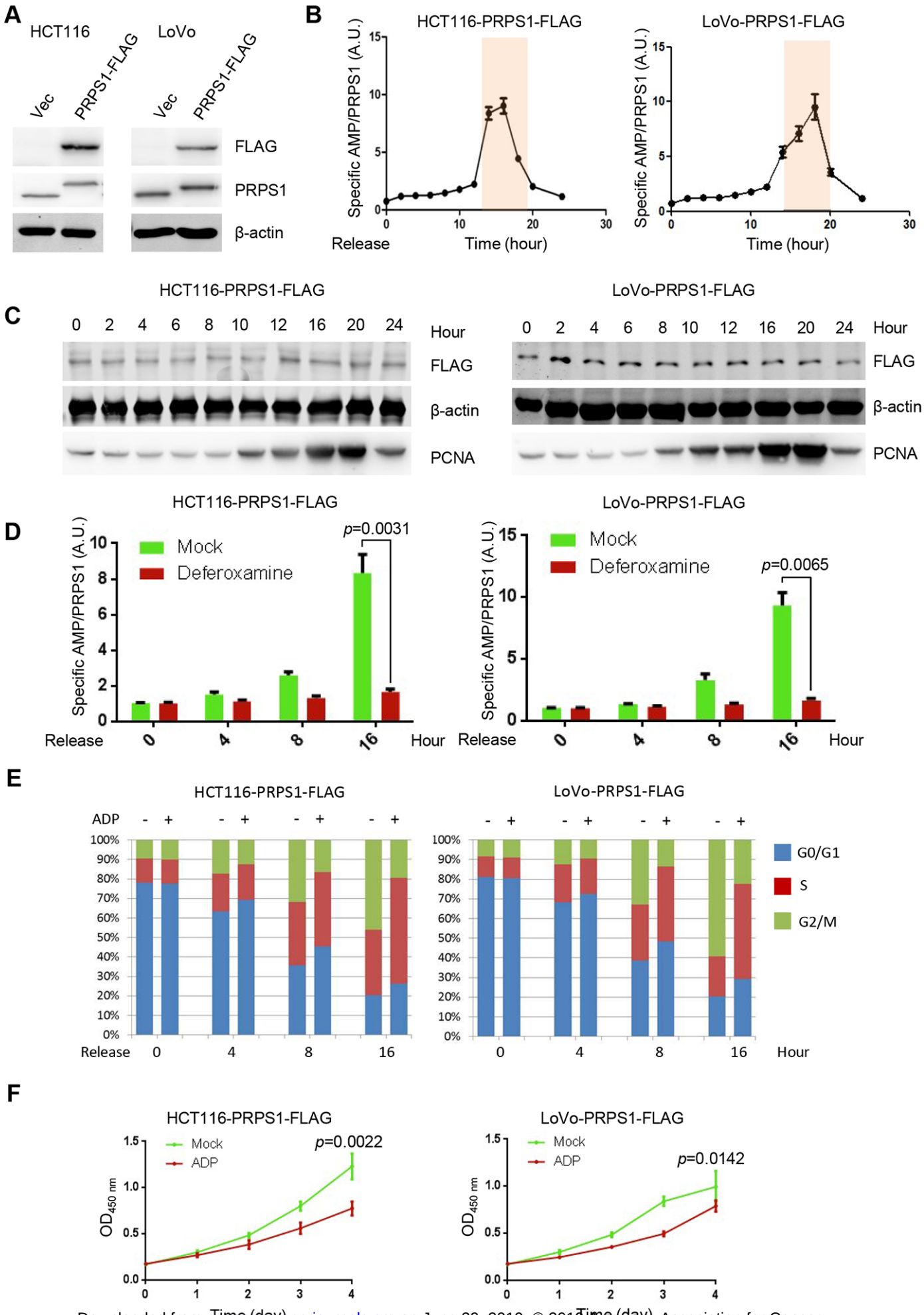

Figure 3

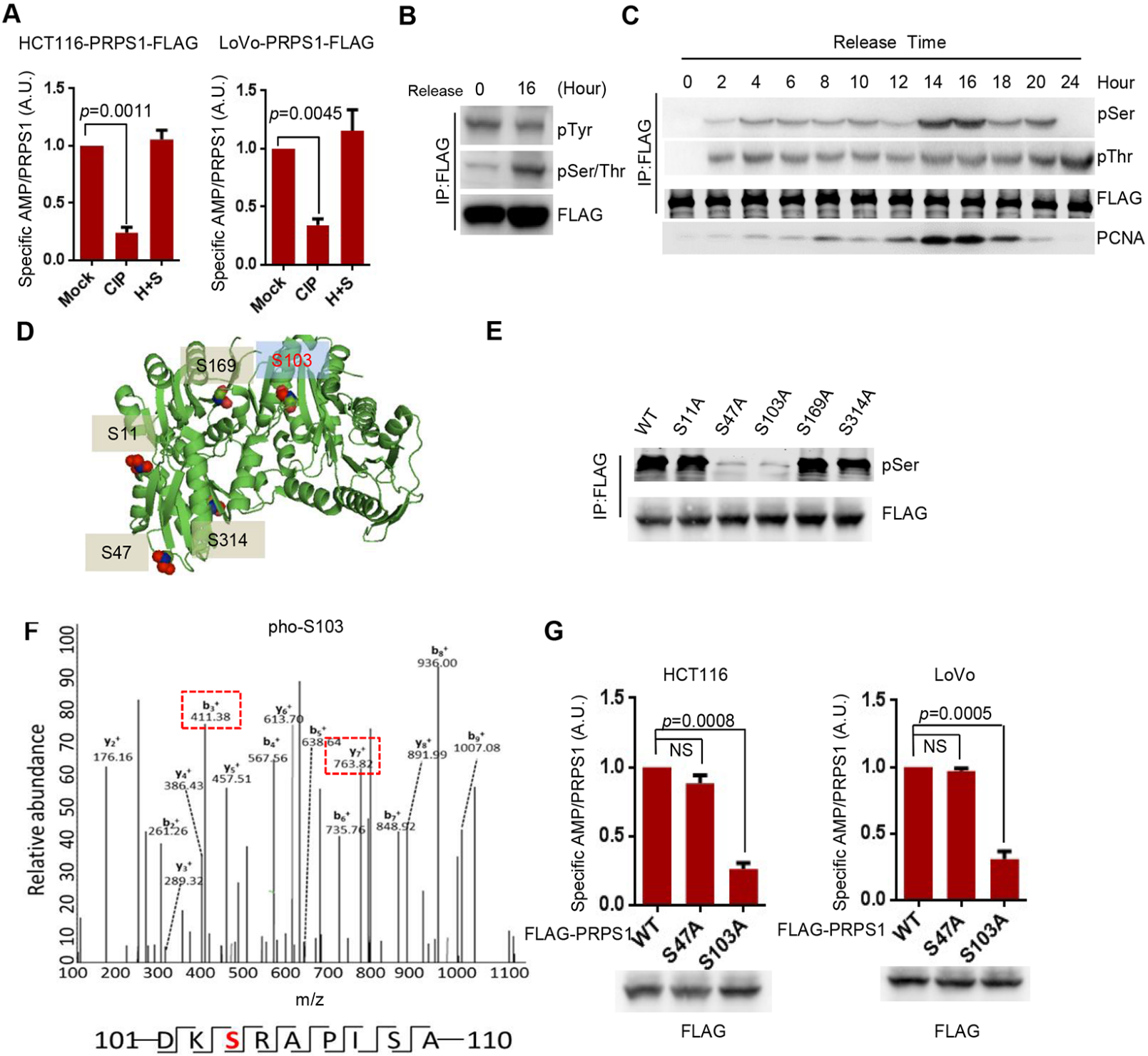

Figure 4

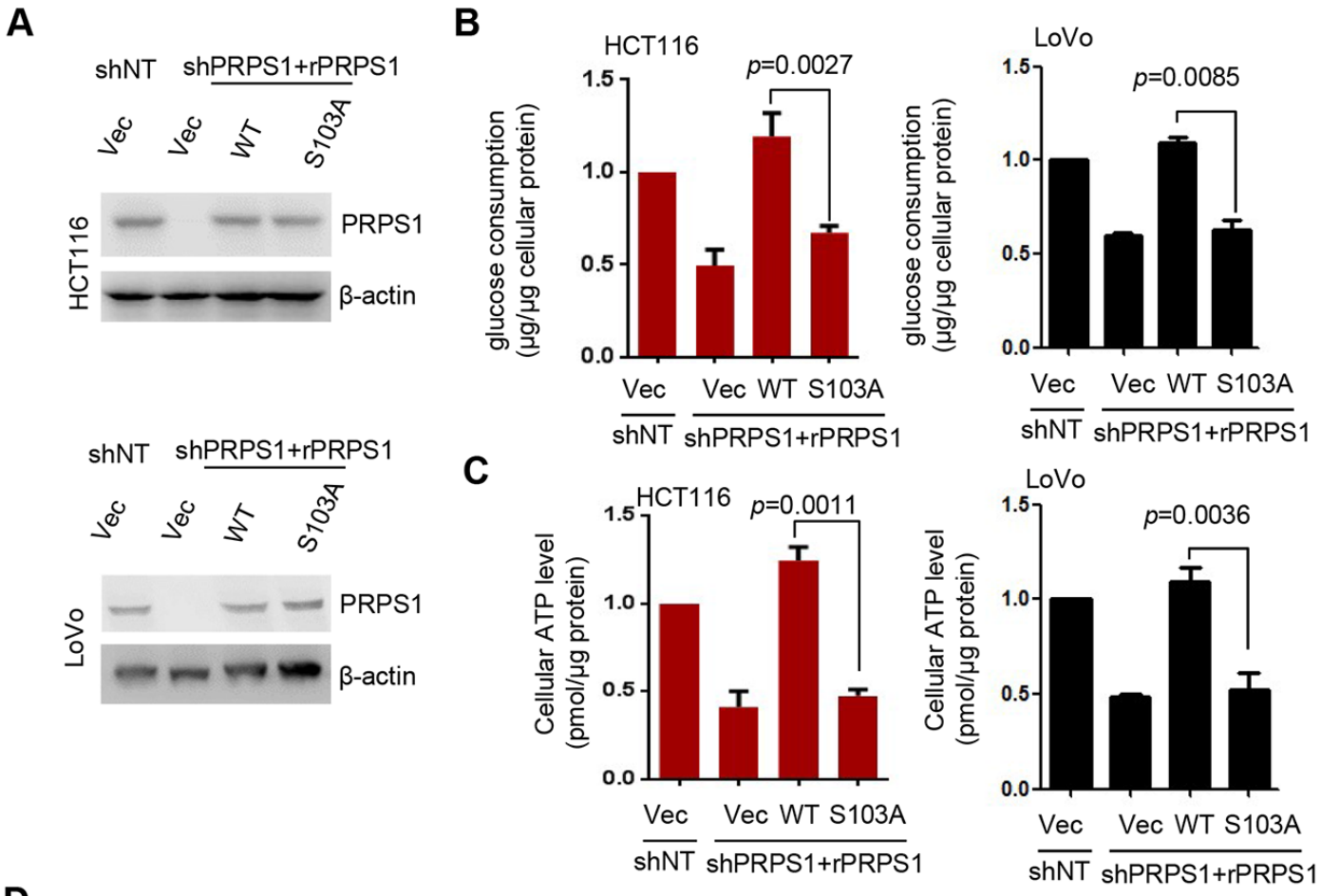

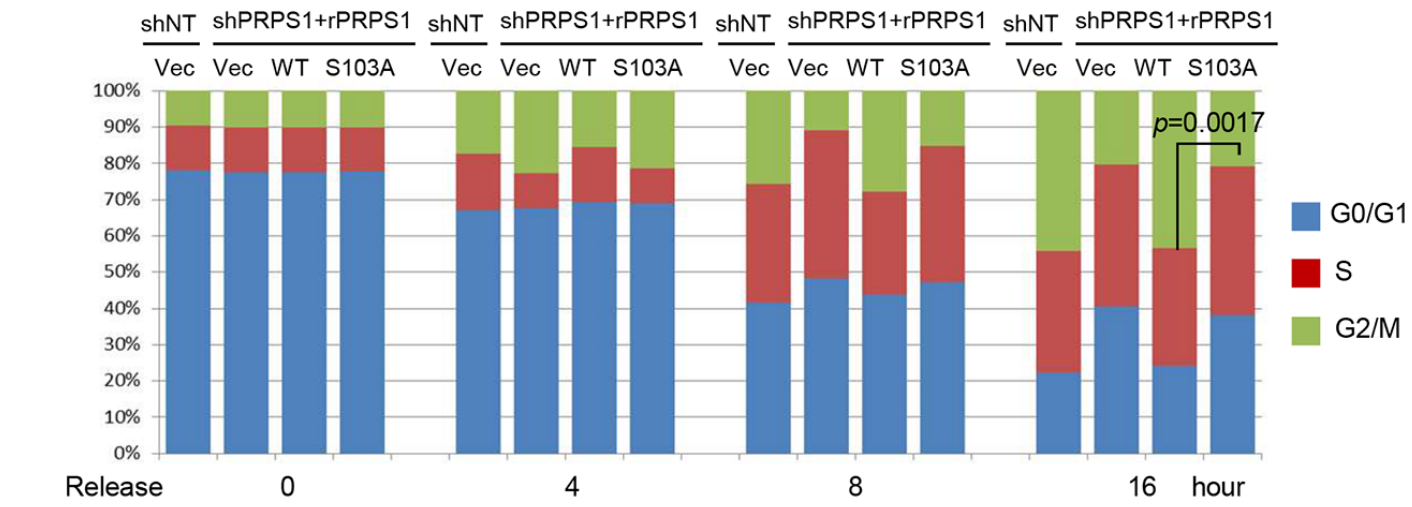

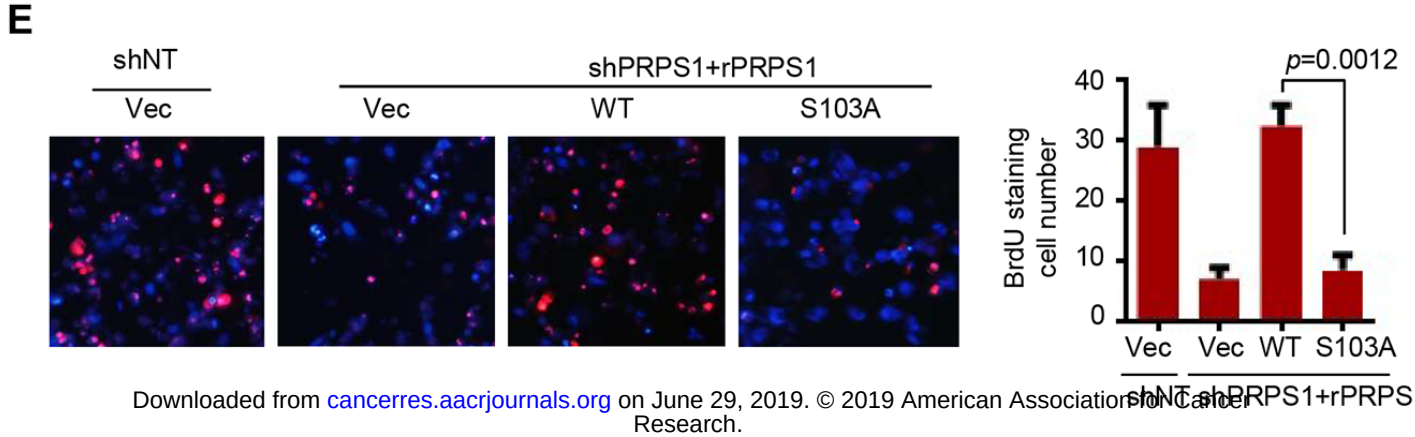

Figure 5

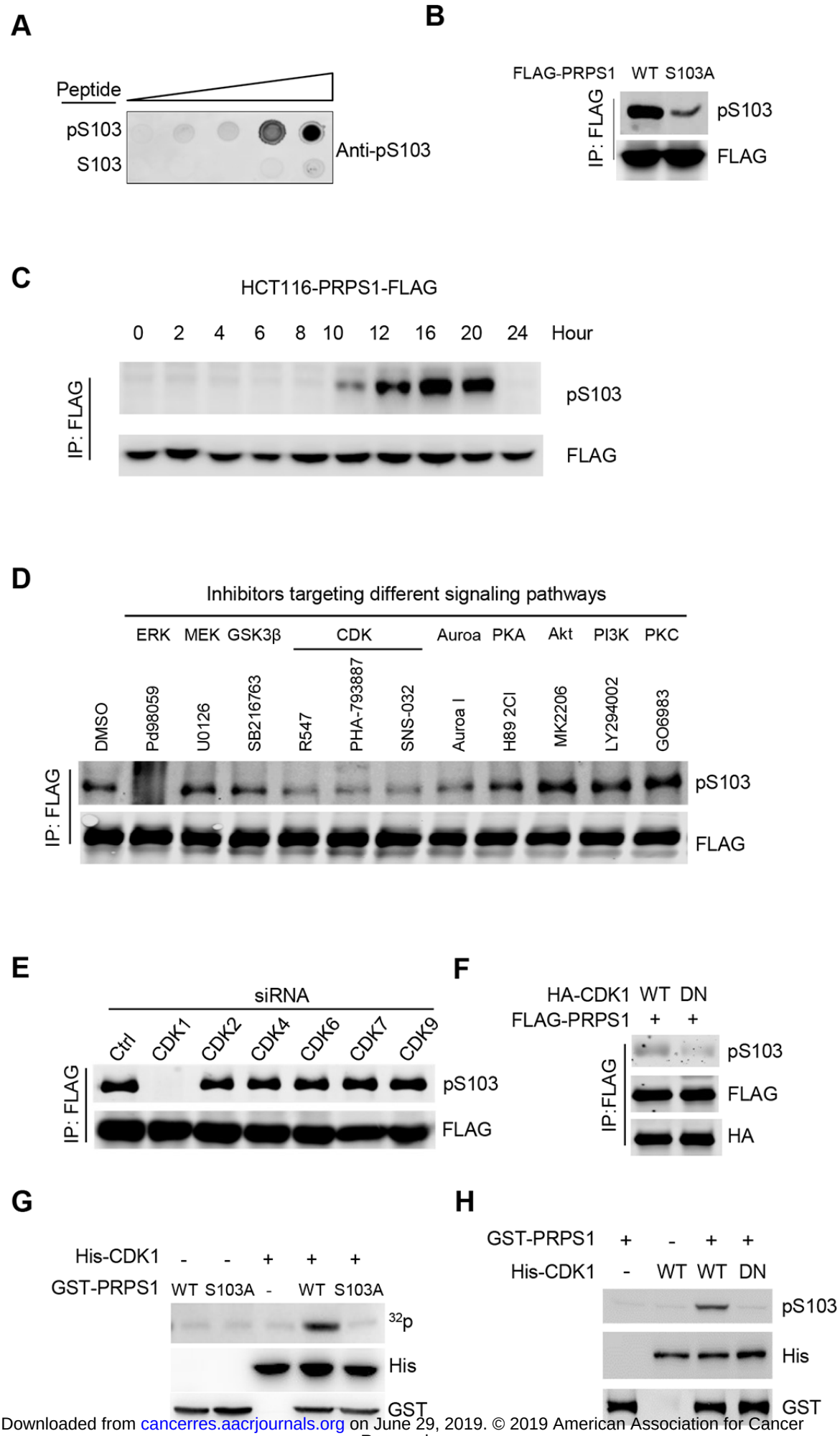

Figure 6

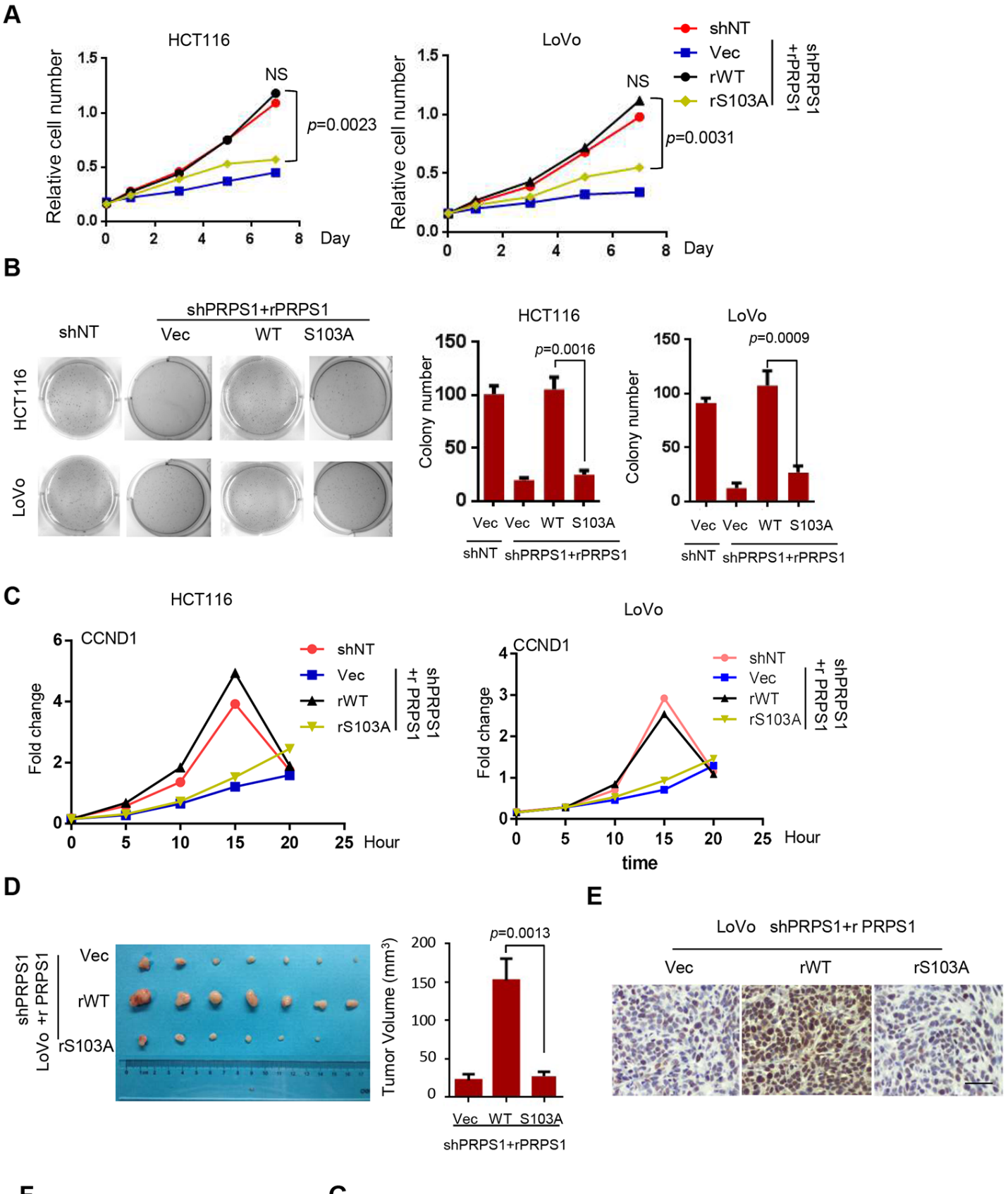

Figure 7

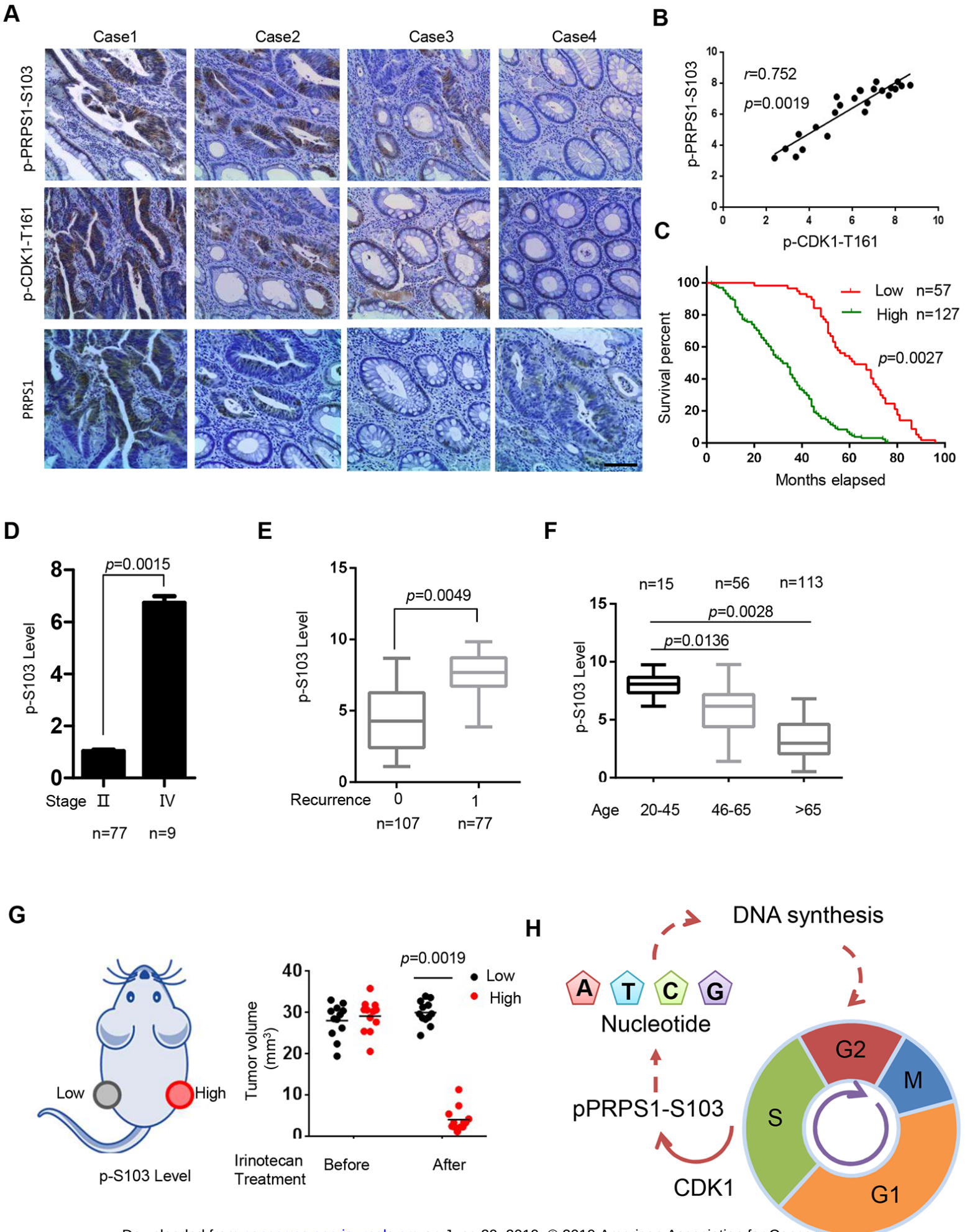

AACR American Association for Cancer Research

Cancer Research

The Journal of Cancer Research (1916–1930) | The American Journal of Cancer (1931–1940)

Cell cycle-dependent phosphorylation of PRPS1 fuels nucleotide synthesis and promotes tumorigenesis

Xiaoqian Jing, Xiong-jun Wang, Tao Zhang, et al.

Cancer Res Published OnlineFirst June 28, 2019.